Disrupted periodic spatiotemporal pattern and dynamic reorganization of its basic states in generalized epilepsy

Journal of Neural Engineering

OPEN ACCESS

RECEIVED
2 April 2025

REVISED
27 July 2025

ACCEPTED FOR PUBLICATION
2 September 2025

PUBLISHED
18 September 2025

PAPER

Disrupted periodic spatiotemporal pattern and dynamic reorganization of its basic states in generalized epilepsy

Junxia Chen[1], Sisi Jiang[1,2,3], Guofeng Ye[1], Zhihuan Yang[1], Changyue Hou[1], Hechun Li[1,3], Haonan Pei[1], Roberto Rodriguez-Labrada[4], Jianfu Li[1,3], Dezhong Yao[1,2,3] and Cheng Luo[1,2,3,5,*]

[1] The Clinical Hospital of Chengdu Brain Science Institute, School of Life Science and Technology, University of Electronic Science and Technology of China, Chengdu 611731, People's Republic of China
[2] Research Unit of NeuroInformation, Chinese Academy of Medical Sciences, 2019RU035 Chengdu, People's Republic of China
[3] China-Cuba Belt and Road Joint Laboratory on Neurotechnology and Brain-Apparatus Communication, University of Electronic Science and Technology of China, Chengdu 610054, People's Republic of China
[4] Cuban Neuroscience Center, La Habana, Cuba
[5] Department of Radiology, The Fourth People's Hospital of Chengdu, Chengdu 610000, People's Republic of China
[*] Author to whom any correspondence should be addressed.

E-mail: chengluo@uestc.edu.cn

Keywords: idiopathic generalized epilepsy, periodic spatiotemporal pattern, default mode network, resting states

Supplementary material for this article is available online

Abstract

Objective. The anti-correlation between the default mode network (DMN) and task-positive network (TPN) is a stable characteristic of normal brain activity. However, in idiopathic generalized epilepsy (IGE), this anti-correlation is often disrupted and strongly associated with epileptic seizures. This study aims to use periodic spatiotemporal patterns (PSTP) analysis to elucidate the relationship between the DMN-TPN anti-correlation and epileptic activity, providing new insights into the neural mechanisms underlying IGE. *Approach.* Resting-state functional magnetic resonance imaging was used to analyze PSTP in both healthy controls and IGE patients. A pattern-finding algorithm was initially applied to identify repeated spatiotemporal patterns, followed by a novel PSTP-finding algorithm to uncover dynamic periodic patterns through analysis of fluctuations in the DMN-TPN anti-correlation. The Hilbert transform was applied to capture the underlying basic states of these periodic patterns. Additionally, the relationship between period length and intrinsic neural timescales (INT) was explored. *Main results.* IGE patients exhibited a reduced DMN-TPN anti-correlation, particularly during TPN-dominant states. Additionally, IGE patients exhibited greater dynamic instability in basic states, marked by more frequent transitions between transitional states. Furthermore, lower correlations between period length and INT were observed in cognitive regions of IGE patients. *Significance.* These findings suggest that dynamic switching between the DMN and TPN in IGE is weaker and less balanced, with disruptions in periodic rhythms linked to cognitive impairments. The proposed PSTP framework provides new insights into the abnormal rhythms of IGE from a spatiotemporal perspective.

1. Introduction

A generalized tonic–clonic seizure (GTCS) is the most clinically prominent subtype of idiopathic generalized epilepsy (IGE), typically characterized by 2.5–5 Hz generalized spike-wave discharges (GSWDs), tonic–clonic movements, and loss of consciousness [1]. These seizures arise from abnormal neuronal synchrony driven by imbalances in excitation and inhibition, disrupted neuronal function, and impaired network connectivity [2]. Increasing evidence suggests that epileptic electrical activity originates from the behavior of propagated brain networks [3–5]. Electroencephalogram-functional magnetic resonance imaging (EEG-fMRI) study has demonstrated suspension of default mode network (DMN) activity during GSWD generation and propagation, implicating DMN involvement in seizure dynamics [6]. However, previous research has largely relied on static connectivity or time-domain analyses [7–9],

overlooking the spatiotemporal dynamics and periodic evolution of DMN activity in IGE. The metastability of brain states maintains spontaneous activity most of the time, with sudden bursts into periods of GSWDs at certain moments. Therefore, it is crucial to study the dynamic spatiotemporal characteristics of brain function in epilepsy patients during the resting state. Furthermore, disrupted interaction between the DMN and task-positive network (TPN) has also been reported [10–12], which was related to cognitive impairment in epilepsy patients [13, 14]. The exploration of the abnormal interactions between DMN and TPN in epilepsy is crucial for a better understanding of the underlying mechanisms of seizures and behavioral disorders.

Studies have suggested that electrophysiological signals exhibit periodic characteristics [15] and that neuronal activity also undergoes slow and periodic modulation on time scales of 1–100 s [16]. These inherent temporal rhythms are accompanied by non-stationary dynamics in large-scale brain networks, including time-varying interactions between core nodes of the DMN and TPN [17, 18]. However, it remains unclear whether there is a dynamic balance (reaching a steady state over time or changing periodically) for this unstable phenomenon. Prior studies have primarily focused on temporal characteristics, while the spatiotemporal evolution of brain dynamics remains underexplored. Yousefi and Keilholz reported a quasi-periodic feature of low-frequency spatiotemporal pattern in the brain [19], which reflects the spatial pattern of infra-slow electrical activity (<0.1 Hz) embedded in the blood–oxygen-level-dependent (BOLD) signal. This might illuminate coordination mechanisms within and between the brain's large-scale networks [20, 21]. The pattern involves dynamic changes in the anti-correlation between DMN and TPN (∼20 s) in BOLD. However, applying a fixed temporal window may obscure individual differences in periodicity. Personalized periodic length may reflect individual variability in DMN-TPN switching speed, potentially linked to regional information retention capacity. Given the periodicity of these patterns, this study could reasonably assume that spatiotemporal patterns might be composed of different basic states of the brain. Basic states of the brain reflect the spatially invariant basis of the brain, involving different brain network interactions.

The 'basic state' proposed in this study is theoretically distinct from traditional transient-state models, such as the hidden Markov model [22] and co-activation patterns [23]. These traditional approaches characterize instantaneous 'snapshots' of brain activity at specific time points, emphasizing transience and discreteness [24, 25]. In contrast, the basic state is grounded in low-frequency (<0.1 Hz), periodic spatiotemporal dynamics of the brain, and captures a more fundamental, spatially invariant basis underlying complex patterns, including the anti-correlated DMN-TPN fluctuations. Rather than focusing on short-lived events, the basic state emphasizes continuous transitions and the global organization of brain dynamics. The basic state recapitulates hallmark features of the default mode-namely, sustained activity fluctuations and a stable spatial configuration-within the broader continuum of whole-brain dynamics [26–28]. This perspective holds promise for unraveling the core mechanisms underlying dynamic balance in the brain, offering a novel perspective for understanding functional network coordination.

To investigate the dynamic periodic spatiotemporal characteristics of IGE, this study first identified personalized periodic spatiotemporal patterns (PSTP) for each participant. Since PSTP reflects the spatiotemporal architecture in the BOLD signal, the study examined its contribution to the BOLD signal. Additionally, the relationship between period length and the intrinsic neural timescales (INT) was also explored. Subsequently, the study explored the basic states of PSTP through phase synchronization (PS) and leading eigenvector analysis, and studied the feature changes of states in IGE. The transition between epileptic states and normal brain states makes the study of dynamics in epilepsy particularly important [29]. An overview of this study is shown in figure 1(A). This study provides a new perspective for exploring the brain mechanisms underlying epilepsy.

2. Materials and methods

2.1. Participants

A total of 100 patients (age = 24.64 ± 8.70 years, 43 females) with GTCS were recruited from the neurology department, the Affiliated Hospital of University of Electronic Science and Technology of China. According to the International League Against Epilepsy [30], the diagnosis of all patients was established by two neurologists. Thirty-three of the 100 patients were drug-naïve first-episode patients. All subjects in this study stopped taking antiseizure medications within 24 h before scanning. None of the patients had seizures before scanning. To provide a neuroimaging reference, 104 demographically matched healthy control (HC) subjects (age = 25.85 ± 7.87 years, 44 females) were also recruited as the HC group. Written informed consent was obtained from all subjects. All study methods and the process design were approved by the local Ethics Committee of University of Electronic Science and Technology of China and followed the declaration of Helsinki (2022LLYJ08). Detailed material on the subjects is shown in table 1.

2.2. Image data acquisition

MRI data were acquired using a 3.0 T MRI scanner (Discovery MR750, GE). All participants were

Table 1. Demographic characteristics of IGE patients and healthy controls.

Characteristic	IGE	HC	*P*-value
Number	100	104	—
Age (year)	24.64 ± 8.70	25.85 ± 7.87	0.296[a]
Sex (M: F)	57:43	60:44	0.920[b]
ASMs (with: without)	67:33	—	—
Age at onset(year)	19.85 ± 9.24	—	—
Illness duration(year)	4.81 ± 6.75	—	—
mFD (mm)	0.113 ± 0.05	0.088 ± 0.04	—

Abbreviations: ASMs: antiseizure medications; mFD: mean frame-wise displacement.

[a] The *p*-value was obtained by a two-sample *t*-test.

[b] The *p*-value was obtained by a χ^2 test.

given foam padding to reduce head motion. The fMRI images were collected using an echo-planar imaging sequence. The scanning parameters were as follows: slices = 35, TR/TE = 2000 ms/30 ms, flip angle = 90°, FOV = 240 mm × 240 mm, matrix size = 64 × 64, thickness = 4 mm, and 255 volumes in each run (each scan takes 8 min and 30 s). Axial anatomical T1-weighted images were attained using a 3-dimensional fast spoiled gradient echo (T1-3D FSPGR) sequence: TR = 6.012 ms, TE = 1.968 ms, FA = 9°, matrix = 256 × 256, FOV = 256 mm × 256 mm, slice thickness = 1 mm, 152 slices without a gap. During scanning, the subjects were instructed to keep their eyes closed and not to fall asleep.

2.3. Image processing

The preprocessing pipelines were consistent with the previous study [31], including the removal of the first five time points, estimation of head motion, slice-timing correction, and boundary-based registration to T1w image. All functional images were then resampled onto the fsaverage surface space. The following pre-processing steps were additionally performed. (1) To further reduce physiological noise and artifacts, the head motion, white matter, cerebrospinal fluid, and global signals were regressed. (2) A band-pass filter (0.01–0.1 Hz) was employed. (3) The spatial dimension was reduced to N (where N is the dimension of the parcellation) cortical parcels, and the time series for each parcel was normalized to zero mean and unit standard deviation. The study used a multimodal brain atlas to parcellate cortical vertices into 360 ($N = 360$) parcels [32].

2.4. Algorithm for finding PSTP

2.4.1. Step 01: detection of repeated spatiotemporal patterns (RSTP)

The pattern-finding algorithm detected the RSTP, which consists of three-dimensional spatial patterns persisting over a continuous period of W timepoints (where W denotes the number of timepoints forming the RSTP). Thus, it captures brain functional spatiotemporal information in a four-dimensional representation (figure 1(B)). The algorithm involves five procedures. (1) The window length was set to W, and a random window was selected as an initial template. The maximum number of possible selections does not exceed L ($L = M-W + 1$, where M denotes the length of the preprocessed time series). To minimize bias, all possible selections were performed, yielding L initial templates for subsequent analyses. (2) To ensure the stability of the final RSTP, the time point with the highest DMN signal in the template was moved to the first position, and the signals of the remaining timepoints were shifted accordingly. The DMN mask was derived from a pre-established group-level mask (see supplementary material). (3) The correlation between the template and each segment was calculated with a step size of 1 TR. Each segment represents a temporally contiguous signal epoch of identical duration to the template. The correlation coefficients were concatenated into a one-dimensional correlation vector. (4) Similar segments corresponding to local maxima exceeding a preset threshold in the correlation vector were averaged to generate a candidate segment. (5) If the similarity between the candidate segment and the template reached 0.9999, the candidate segment was designated as a RSTP. Otherwise, the candidate segment was used to update the template, and procedures 2–5 were iterated until convergence was achieved. To ensure the non-arbitrariness and adaptability of the preset threshold, the correlation threshold for the first three iterations was 75% of the correlation vector, and 85% for subsequent iterations, with a maximum of 15 iterations. If convergence was not achieved within 15 iterations, the result based on this initial template was excluded from further analysis. Consequently, up to L RSTPs could be obtained, assuming all initial templates successfully converged.

2.4.2. Step 02: searching for representative repeated pattern (RRP)

L' repeated patterns satisfying predefined screening criteria were first identified from L RSTPs. Then, a RRP closest to a DMN-to-TPN transition was selected from L' RSTPs (see supplementary material for details). In brief, the RRP starts with high DMN

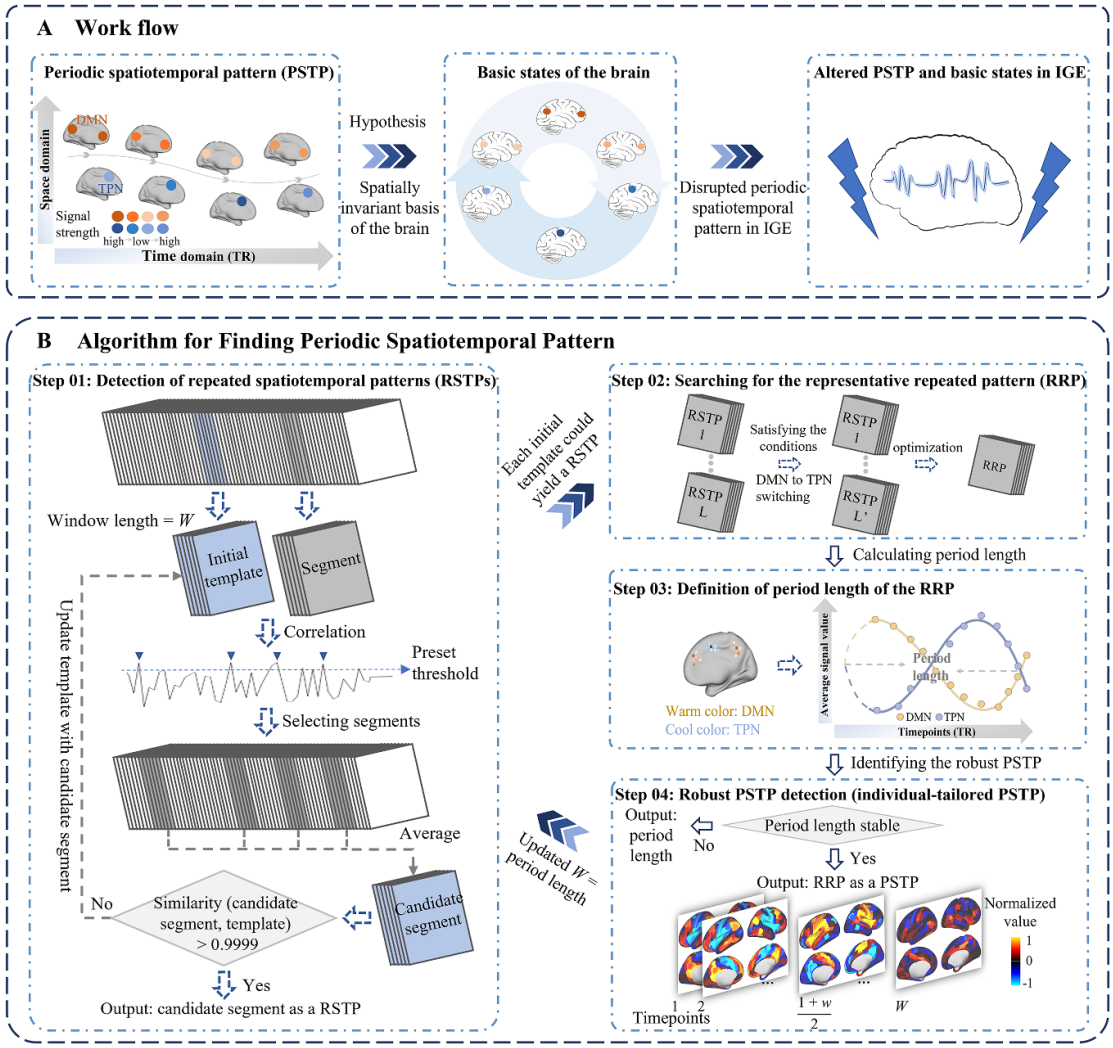

Figure 1. Workflow and schematic of analytical processing based on periodic spatiotemporal pattern (PSTP). (A) The PSTP reflects the spatial changes over time of the default mode network (DMN) and task-positive network (TPN). This study assumes that spatiotemporal dynamic changes are based on a state-invariant spatial foundation. Finally, it was applied to patients with idiopathic generalized epilepsy (IGE) to explore the spatiotemporal heterogeneity. (B) Looking for a robust PSTP. Firstly, RSTP were iteratively identified using a pattern-finding algorithm until the candidate segment stabilized and was output as the final RSTP (Step 01). Each random initial template can result in a RSTP. Next, L' ($L' < L$) repeated patterns were extracted from the L (L denotes the number of random initial template selections) RSTPs that matched the DMN to TPN switching. Then the mean correlation between L' RSTPs was calculated (resulting in L' correlation coefficients), and the RSTP with the highest correlation was defined as the representative repeated pattern (RRP). This indicates that the RRP is most like the other RSTPs (Step 02). Subsequently, the period length was defined by the inverse correlation between the DMN and TPN signals in RRP (Step 03). Then, if the period length differed from the previous iteration, the window length (W) was updated, and Step 01 was repeated. When the period length stabilized across iterations, the final individual-tailored PSTP was obtained in Step 04.

activity, which gradually decreases, while TPN activity increases from a low level. This is followed by a reversal where DMN activity rises and TPN activity declines.

2.4.3. Step 03: definition of period length of the RRP

The procedures to define the periodic length of the RRP were as follows. (1) The average signals of DMN and TPN in RRP were extracted, and polynomial fitting was performed, respectively. (2) The point where the fitting signals of DMN and TPN had the smallest difference and were closest to the first time point of the pattern was considered the starting point of the period; meanwhile, the point where the fitting signals of DMN and TPN had the smallest difference and were closest to the last time point of the pattern was used as the endpoint of the period (as shown in figure 1(B), with a detailed description in supplementary figure S1). (3) The period length was defined as the number of timepoints between the starting point and the endpoint. For more details, please refer to supplementary material.

2.4.4. Step 04: robust PSTP detection

Two types of PSTP were explored for each subject by adjusting the continuous time length W: The fixed PSTP and the individual-tailored PSTP.

Fixed PSTP: W was set to 10 TRs, and then the above algorithm was applied to obtain RRP. The RRP was considered the fixed PSTP.

Individual-tailored PSTP: The PSTP-finding algorithm was used to identify a stable individual-tailored PSTP. (1) The window length W was set to 10 TRs to detect the RRP and estimate its period. (2) This period was used as the new W, and the pattern-finding algorithm was applied again to detect the PPR and period length under this condition. This process (procedure (2)) was iterated until the period length of the RRP remained unchanged. The RRP and period length of RRP obtained from the last iteration were defined as a robust individual-tailored PSTP and period length of the individual-tailored PSTP, respectively. Notably, the final number of timepoints (W) may vary across individuals, preserving personalized periodic features.

For both within-group and between-group comparisons of PSTP-related metrics, normality tests were conducted for each variable. Based on the results, appropriate statistical methods were selected. For normally distributed data, the t-test was used. For non-normally distributed data, the Mann–Whitney U test was applied for independent samples, and the Wilcoxon signed-rank test was used for paired samples.

For fixed PSTP, statistical analysis was performed within each group. Simultaneously, the squared differences between DMN and TPN timecourses were compared between the control and IGE groups, with age, sex, and head motion controlled for. Statistical significance was determined using family-wise error (FWE) correction with $p < 0.05$.

Following this, to quantify the variation of the PSTP over time, the strength, frequency, and interval time of the PSTP occurrence over time were compared between groups. The strength was defined as the mean of the supra-threshold local maxima in the correlation vector of the PSTP. The frequency was defined as how often the supra-threshold local maxima occur. Meanwhile, the interval time was considered as the mean interval time between successive local maxima.

2.5. Spatiotemporal characteristics of PSTP

2.5.1. Spatial characteristics: the contribution of PSTP to BOLD

Two approaches were used to examine the contribution of PSTP to BOLD signals. On the one hand, the study focused on quantifying the strength of PSTP while controlling for its occurrence frequency across participants. Specifically, each participant's PSTP was sliding-correlated with the BOLD signal to generate a correlation vector. To ensure a consistent number of suprathreshold time windows, thresholds were defined using individual percentiles of the correlation vector, ranging from the 15th to 95th percentile in 10% increments. PSTP strength at each threshold was defined as the mean correlation value of time windows exceeding that threshold. Group differences in PSTP strength were assessed at each threshold level.

On the other hand, to explore the role of this spatiotemporal pattern in the process of generating functional connectivity (FC) in the brain, the relationship between FC and PSTP was evaluated. First, the average timecourse of cortical vertices within each of Yeo's networks [33] was extracted to calculate FC between networks using Pearson correlation. Next, each subject's FC matrix underwent a Fisher's z-transformation. FC was also calculated for the functional scans after regressing the PSTP using scan-wise regression (see supplementary material). Regression was necessary as it allows the study of PSTPs' contribution to FC by attenuating their effect on the BOLD signal. Finally, within-group analyses and between-group comparisons were performed (False Discovery Rate, FDR, $p < 0.05$), with age, sex, and head motion as covariates. Notably, the statistical tests were conducted before and after regression to the PSTP.

2.5.2. Temporal characteristics: association analysis between period length and INT

To explore whether the period length relates to the ability of brain regions to maintain information, the relationship between period length and INT was assessed using Spearman correlation. INT refers to temporal durations (i.e. timescales) of the brain's neural activity [34], calculated here using the method proposed by Raut *et al* [35]. Firstly, the autocovariance function (ACF) was computed for each brain region. ACF assesses the self-similarity of BOLD signals, as shown in equations (1) and (2):

$$c_{x_b}(\Delta) = \sum_{g=1}^{N_b-\Delta} x_b(g+\Delta) \times x_b(g) \tag{1}$$

$$c_x(\Delta) = \frac{1}{N_\Delta} \sum_{b=1}^{B} c_{x_b}(\Delta) \tag{2}$$

where Δ represents the lag time in TRs, b indexes blocks of consecutive frames within the session, g indexes frames within the block, and $x_b(g)$ denotes the signal at timepoint g in block b. N_b is the number of frames within the block, $c_{x_b}(\Delta)$ represents the autocorrelation function at lag Δ within block b. Moreover, N_Δ is the number of timepoints used for estimating the ACF at a given lag, B is the total number of blocks, and $c_x(\Delta)$ is the overall autocorrelation across all blocks.

In this study, the lag time was set to 12 s ($\Delta \in [-6, 6]$). Then, the exact abscissa corresponding to the autocorrelation value of 0.5 (i.e. half the full width at half maximum of ACF) was estimated by calculating the zero point of the spline curve fitted to ACF. Next, this coordinate value was then multiplied by the TR, thus resulting in the INT of a brain region. Subsequently, Spearman correlation calculation was performed between INT and the period length of individual-tailored PSTP. Within-group correlations were adjusted for false discovery rate (FDR, $p < 0.05$).

The correlations were compared between IGE and the controls by permutation test (5000 times, $p < 0.05$). Finally, to further decode the cognitive implications of the regions exhibiting IGE-related alterations in correlation between INT and period length, a functional meta-analysis using the Neurosynth database was performed [36].

2.6. Basic states identification based on PSTP

2.6.1. Instantaneous PS analysis based on Hilbert transform

The instantaneous PS [37] was estimated to obtain a time-resolved PS matrix, enabling the analysis of spatiotemporal interactions between various brain regions in an extremely short time [38]. To compute PS, BOLD signals of all parcels in the PSTP ($N \times W$; N, number of parcels; W, number of timepoints) were first Hilbert transformed into an analytic signal as shown in equation (3):

$$X(w) = A(w) \times \cos(\theta(w)), \quad (3)$$

where $A(w)$denotes the instantaneous amplitude, reflecting the strength of the oscillation, and $\theta(w)$ represents the instantaneous phase, describing the signal's position within its oscillatory cycle (e.g. peak, trough, rising, or falling phase) at time w. This decomposition enables a fine-grained analysis of neural dynamics by separating signal magnitude from its phase timing, allowing subsequent calculation of PS, phase-amplitude coupling, or temporal alignment across brain regions.

To compute PS, the phase of each parcel was extracted from the analytic signal, and the PS matrix was constructed by computing the cosine of the phase difference between all pairs of parcels n_1 and n_2 ($n_1 = 1, \ldots, N$; $n_2 = 1, \ldots, N$) at each timepoint w ($w = 1, \ldots, W$). The PS at time w between two parcels was calculated as shown in equation (4):

$$\mathrm{iPS}(n_1, n_2, w) = \cos(\theta(n_1, w) - \theta(n_2, w)), \quad (4)$$

where $\theta(n_1, w)$ and $\theta(n_2, w)$ are the instantaneous phases of parcels n_1 and n_2 at time w, respectively. The resulting PS matrix is a three-dimensional tensor of shape $N \times N \times W$, capturing pairwise phase relationships over time.

Each value of $\mathrm{PS}(n_1, n_2, w)$ ranges from -1 to 1: a value of 1 indicates perfect PS (i.e. parcels oscillating in-phase), whereas -1 indicates complete anti-PS. A value near 0 implies no consistent phase relationship at that timepoint. This formulation enables dynamic assessment of functional integration or segregation across brain regions.

2.6.2. Leading eigenvector analysis

To reduce the dimensionality of the phase space (from $\frac{N(N-1)}{2}$ to N), the leading eigenvector analysis method was applied. The leading eigenvector $V_1(w)$ (the dimension was $N \times 1$) of each PS matrix was extracted from the matrix that was the eigenvector corresponding to the maximum eigenvalue. The $V_1(w)$ captures the main orientation of the fMRI signal phase overall anatomical areas, and focuses on the dominant connectivity pattern of PS at time w, rather than the whole upper triangle, it is more robust to high-frequency noise [39].

To determine the discrete number of basic brain states, clustering analysis was applied to all leading eigenvectors ($S \times W$, where S is the number of participants) across participants and frames of the PSTPs using K-means clustering. K (the number of clusters) ranged from 2 to 10, with 300 repetitions. Each clustering centroid ($N \times 1$) represents a basic state of the brain, with positive weight indicating positive co-modulation and negative weight indicating negative co-modulation between cerebral regions. Hence, each frame of the PSTP was assigned a cluster (or a basic state), resulting in a discrete time series $x(w)$ for each subject, where $w = 1, \ldots, W$, where each discrete value (between 1 and K) indicates the active state at that frame of the PSTP [40].

To investigate the changes in basic states with PSTP, the three indicators were included in this study. (1) The fraction time $f_{\mathrm{state}\,k}$ of each state was defined as the percentage of frames during which the state was active to the total time (W). (2) The dwell time $d_{\mathrm{state}\,k}$ of each state was defined as the average length of frames of all segments in which the state occurred continuously or remained active. (3) Finally, the transition probability $T_{\mathrm{state}\,i \to j}$ was given by the proportion of the number of transitions from basic state i to j to the total number of possible transitions ($W - 1$). Significant differences in these measures were tested between the controls and IGE.

Additionally, the current study used the intraclass correlation coefficient to determine the homogeneity of states between individual-tailored and fixed PSTP. Finally, significance testing of correlations between states was assessed via spin permutation tests with 1000 repetitions.

2.7. PSTP validation and comparison with traditional approaches

To validate and evaluate the specificity of the proposed PSTP method, this study conducted the following analyses: (1) to ensure that the observed PSTP arises from the intrinsic temporal structure rather than random phenomena, a surrogate dataset was generated with the same mean, variance, and frame count as the real data; (2) to better characterize and validate the PSTP method, quasi-PSTP [19] was calculated in both the HC and IGE groups, and compared with the PSTP. (3) a comparison was made with the traditional sliding window dynamic FC (dFC) method to evaluate its performance in terms of time resolution, noise tolerance, and

pathological specificity. Detailed descriptions can be found in supplementary material.

2.8. Sensitivity and stability analysis

To assess whether the basic brain states derived from the fixed PSTP were influenced by the time series length, a sensitivity and stability analysis was performed. Specifically, the time series was first halved and then progressively extended in increments of 5 or 10 time points. At each length, the fixed PSTP and corresponding basic brain states were recalculated using the same analytical pipeline. Details of the sensitivity and stability analysis were provided in supplementary material.

3. Results

3.1. PSTP

DMN and TPN maps were generated by locating areas strongly correlated or anti-correlated with the posterior cingulate cortex, respectively (supplementary material, figure S2). Robust, individual-tailored PSTPs were identified in 88 HC and 74 IGE patients. Moreover, each subject exhibited unique period lengths (supplementary material, figure S3), with a median duration of 20 s (10 timepoints).

One-sample t-test within each group revealed similar fixed PSTPs ($W = 10$ TRs) in IGE and HC (figure 2(A)), demonstrating consistent patterns of network activation and deactivation (see supplementary videos 1 and 2). The resulting T values were normalized for visualization and group-level comparison. The spatiotemporal patterns in both groups revealed a DMN/TPN switch (figure 2(B)). Interestingly, the switching process in the control group could be characterized by four temporally ordered states, representing distinct phases of network dominance: TPN-ascendant (timepoints 1–3), TPN-dominant (timepoints 4, 5), DMN-ascendant (timepoints 6–9), and DMN-dominant (timepoints 10).

Although the PSTPs were similar between groups, the DMN-TPN relationship within each state differs. The squared difference between their time courses at each time point revealed significant differences in magnitude (two-sample t-test, FWE corrected, $p < 0.05$) (figure 2(B)). There was one phase where the square variance of IGE and HC was significantly decreased, namely the TPN-dominant states (timepoint 4: $t = -4.46$, $p < 0.001$). Additionally, DMN-ascendant states were significantly increased (timepoint 6: $t = 3.72$, $p < 0.001$; timepoint 7: $t = 4.19$, $p < 0.001$).

To evaluate the disturbance of PSTPs in diseases, this study quantified PSTPs and conducted between-group statistical comparisons using a non-parametric Mann–Whitney U test (figure 3(A) and (B)). The results of exploring two spatiotemporal patterns were consistent, showing a decreased frequency of PSTPs in the patients with IGE relative to HCs (fixed PSTP: $z = -4.96$; $p < 0.001$; individual-tailored PSTP: $z = -4.73$; $p < 0.001$). However, the strength of PSTPs in IGE patients (fixed PSTP: $z = 3.81$; $p < 0.001$; individual-tailored PSTP: $z = 3.38$; $p < 0.001$) and interval time increased (fixed PSTP: $z = 5.27$; $p < 0.001$; individual-tailored PSTP: $z = 4.44$; $p < 0.001$).

3.2. Spatiotemporal characteristics of PSTP

3.2.1. Spatial characteristics: the impact of PSTPs on BOLD

To assess the contribution of PSTP to BOLD signals while controlling for occurrence frequency, percentile-based thresholds were applied to each participant's sliding correlation vector. Thresholds ranged from the 15th to the 95th percentile by 10% increments, ensuring a consistent number of suprathreshold time windows across individuals. PSTP strength was calculated as the mean correlation value of suprathreshold windows at each threshold. Compared to HC, patients with IGE showed significantly increased PSTP strength across all thresholds (two-sample t-test, $p < 0.001$).

In addition, to evaluate the contribution of PSTP to FC, group differences in inter-network FC were compared before and after regressing out the PSTP using two-sample t-test. Inter-network FC statistical results were shown in figures 3(C)–(E). The upper triangles of all matrices showed the results before regressing out the PSTP, while the lower triangles showed the results after regression. Before PSTP regression (figure 3(E)), widespread differences in FC were observed between the IGE and control groups. Individuals with IGE showed significantly stronger connectivity between DMN and dorsal attention network (DAN), ventral attention network (VAN), and frontal–parietal network (FPN) ($t_{\mathrm{DMN-DAN}} = 3.91$, $p < 0.001$; $t_{\mathrm{DMN-VAN}} = 2.74$, $p = 0.007$; $t_{\mathrm{DMN-FPN}} = 4.46$, $p < 0.001$). Additionally, increased FC was observed between FPN and limbic network (LN) and visual network (VN), as well as between DAN and VN, and between VAN and LN ($t_{\mathrm{FPN-LN}} = 2.37$, $p = 0.019$; $t_{\mathrm{FPN-VN}} = 2.42$, $p = 0.016$; $t_{\mathrm{DAN-VN}} = 4.69$, $p < 0.001$; $t_{\mathrm{VAN-LN}} = 2.31$, $p = 0.023$). In contrast, decreased FC was found between VAN and VN, VAN and DAN, and between the sensorimotor network (SMN) and both DAN and VN ($t_{\mathrm{VAN-VN}} = 2.32$, $p = 0.022$; $t_{\mathrm{VAN-DAN}} = -4.92$, $p < 0.001$; $t_{\mathrm{SMN-DAN}} = -2.75$, $p = 0.007$; $t_{\mathrm{SMN-VN}} = -2.35$, $p = 0.020$). However, after regressing out PSTP, between-group FC differences were substantially diminished. Notably, only the DMN-FPN connectivity remained significantly elevated in IGE patients ($t_{\mathrm{DMN-FPN}} = 3.81$, $p < 0.001$) (figure 3(E)). These findings were consistent with analyses conducted at the parcel level ($N = 360$ parcels; see figure S4 in supplementary material).

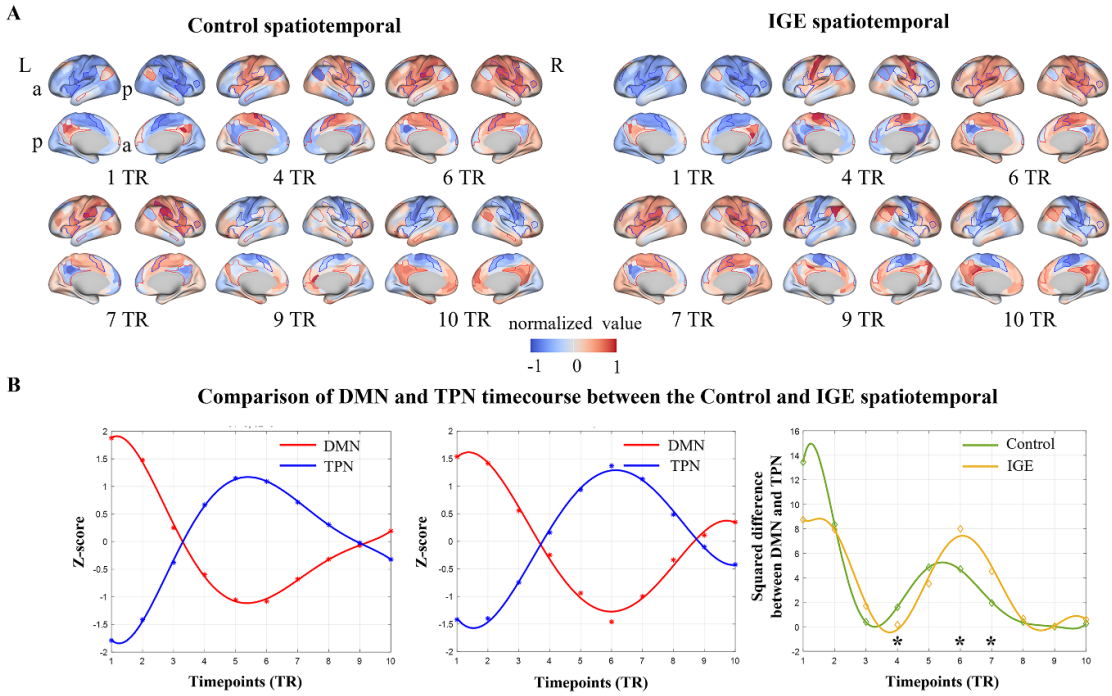

Figure 2. (A) The fixed spatiotemporal patterns of the controls (left) and IGE (right). The normalized value of T value from one-sample t-test was displayed. The red border represents default mode network (DMN), and the blue represents the task-positive network (TPN). (B) Timecourse of the DMN and TPN during spatiotemporal patterns, with the controls shown on the left and IGE in the middle. Note that each asterisk (*) represented the average time signal of DMN or TPN at each time point, and the average signals were normalized by Z-score. The comparison of the square of the differences between DMN and TPN time courses at each timepoint, both in the controls and IGE (right), was performed using a two-sample t-test. Note that each diamond represents the square of the differences at each time point, and each asterisk indicates FWE-corrected significance at $p < 0.05$. All lines were the result of polynomial fitting. Abbreviations: L: left; R: right; a: anterior; p: posterior.

3.2.2. Temporal characteristics: correlation between period length and INT in IGE

The left panels of figure 4(A) and (B) showed that the high INTs were primarily in VN, DMN, and FPN regions, while low INTs were observed in SMN and LN, both in HC and IGE groups. Moreover, the correlation between period length and INT within each group showed significant positive associations mainly in the DMN-related and TPN-related brain regions (FDR-corrected, $p < 0.05$) (as shown in the right image of figure 4(A) and (B)). IGE patients exhibited weaker correlations than HC in higher-order cognitive regions (figure 4(C)) (left hemisphere: 8Av: $p = 0.006$; 46 area: $p = 0.003$; PF: $p = 0.025$; TE1a: $p = 0.022$; right hemisphere: TE2p: $p = 0.032$; 23d: $p = 0.047$; VMV2: $p = 0.043$; STSva: $p = 0.037$). No significantly increased correlation was observed in GTCS relative to HC (permutation test, 5000 times).

NeuroSynth meta-analysis [36, 41] further demonstrated that these impaired correlation regions were functionally associated with advanced cognitive processes, including engagement, language, retrieval, and task performance (figure 4(D)).

3.3. Basic states of the brain

This study characterized the basic states of the brain of the fixed PSTP. The $K = 6$ was ultimately selected (see figure S5 in supplementary material) by Silhouette coefficient. The patterns of the six cluster centers (that is, the six basic states of the brain) corresponding to the fixed PSTP were shown in figure 5. Spatially, each state reflected distinct functional network configurations. Importantly, 4 of the 6 states were grouped into two pairs (state 2 and state 3; state 5 and state 6), and the correlation coefficient between state 2 and state 3 was −0.97, and between state 5 and state 6 was −0.95. Moreover, each pair was dominated by opposite phase-synchronous modes. Specifically, state 2 was mainly composed of positive co-modulation in DMN and FPN, as well as negative coupling in SMN, VAN, and VN. In other words, the connections of SMN, VAN, and VN to DMN and FPN were anti-correlated. State 3 exhibited the inverse pattern. In addition, state 1 consisted of an in-phase mode including VN/ DMN regions and VAN/ SMN anti-phase mode. Relatedly, state 5 was like state 1, but in addition to VN and DMN, the in-phase mode also included FPN. Meanwhile, state 6 was the opposite of state 5. State 4 was dominated by VN/SMN positive co-modulation and VAN/ FPN negative co-modulation. It was worth noting that states 2 and 3 were defined as two poles according to the goodness-of-fit (supplementary material for details) with the DMN template, where state 2 was the most advantageous pole of DMN, and state 3 was the opposite pole. The remaining states were

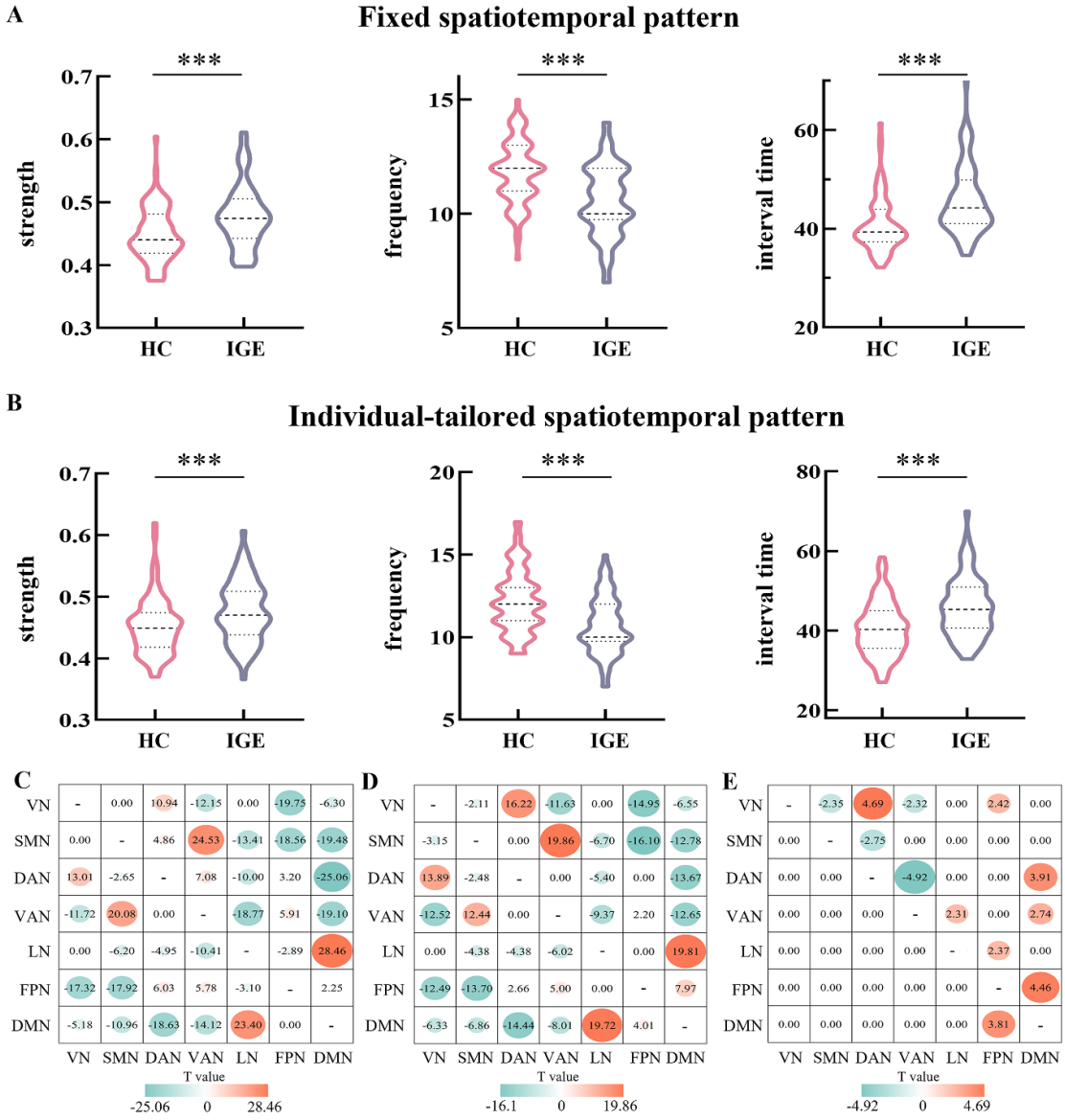

Figure 3. Quantitative metrics of fixed (A) and individual-tailored (B) periodic spatiotemporal patterns (PSTPs), including strength, frequency, and interval time. (C) Bottom-left: one-sample *t*-test of functional connectivity (FC) between networks in the control group after regression of PSTPs. Top-right: one-sample *t*-test of FC between networks in the control group before regression. (D) Bottom-left: the results of FC between networks in the IGE group after regression of PSTPs. Top-right: the FC between networks in the IGE group before regression. (E) Bottom-left: significant differences in FC between the control and IGE groups after regression of PSTPs. Top-right: significant differences in FC between the control and IGE group before regression. The size and color of the circle were consistent with the *T* value. *T* values surviving significance thresholds (one-sample: $p < 0.05$; two-sample: FDR corrected $p < 0.05$) were set to 0. Diagonal autocorrelations were denoted by '-'. Notes: * $p < 0.05$; ** $p < 0.01$; *** $p < 0.001$.

considered transition states. Temporally, based on the propagation mode of DMN to TPN in PSTP, these six states depicted different moments of DMN and TPN. Among them, state 2 represented the most active state of DMN (DMN-active); states 1 and 5 represented the states before and after the moment of the DMN-active, namely DMN-pre and DMN-post, respectively. Similarly, state 3 represented the most active state of TPN (TPN-active); states 4 and 6 represented the states before and after the moment of the TPN-active, namely TPN-pre and TPN-post, respectively. The result of the individual-tailored pattern was almost consistent with the fixed periodic pattern. Ultimately, intraclass correlation coefficients of each corresponding state were greater than 0.96 (spin permutation tests, $p < 0.001$).

Next, this research explored how epilepsy affects these basic state features. Mann–Whitney *U* test showed that the fraction time and dwell time of state 1 were both decreased ($f_{\text{state 1}}$: $z = -3.65$, $p < 0.001$; $d_{\text{state 1}}$: $z = -3.39$, $p < 0.001$) for fixed PSTPs in patients, while states 5 and 6 showed increased presence ($f_{\text{state 5}}$: $z = 2.95$, $p = 0.003$; $f_{\text{state 6}}$: $z = 2.64$, $p = 0.008$; $d_{\text{state 5}}$: $z = 2.83$, $p = 0.005$; $d_{\text{state 6}}$: $z = 2.51$, $p = 0.012$) in figure 6(A). This study also explored the transition probability from a given state to another

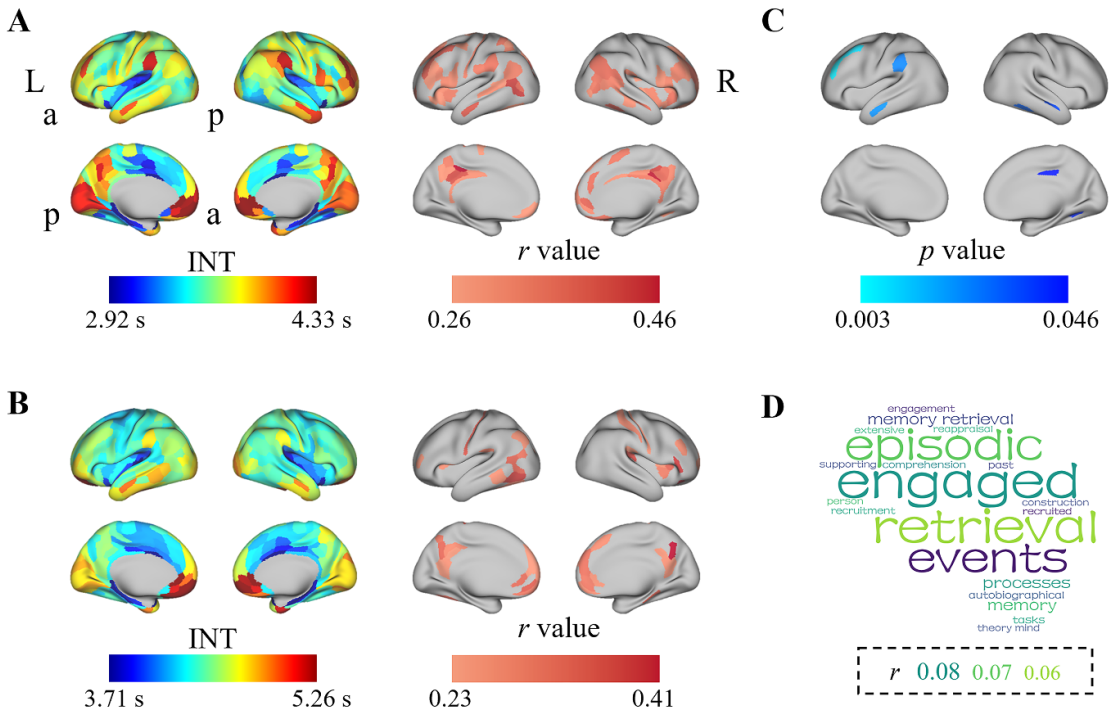

Figure 4. (A) The results in HC. (B) The results in IGE. Left: intrinsic neural timescales (INT). Right: the correlation between the period length of individual-tailored PSTP and INT (FDR, $p < 0.05$). (C) The significant p-value corresponds to the group differences in the correlation between IGE and HC (permutation test, $p < 0.05$). The blue represents the decreased r value of IGE compared with HC. (D) Cognitive terms associated with the regions that exhibited a lower (blue) correlation between the period length of individual-tailored PSTP and INT. Font size has been scaled to reflect the correlation coefficient between the group differences map and the meta-analytic map of that term generated by Neurosynth. Abbreviations: INT: intrinsic neural timescales; left; R: right; a: anterior; p: posterior.

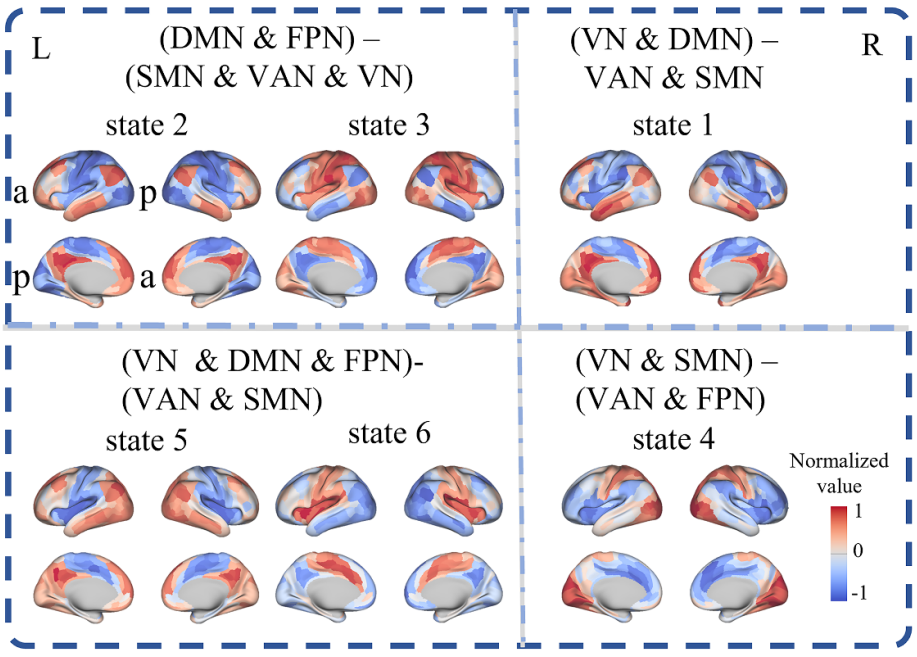

Figure 5. Six basic states of the brain correspond to the fixed periodic spatiotemporal pattern. From a spatial perspective, six basic states captured the interplay of different cortical networks, i.e. each state was characterized by specific functional networks. Moreover, 4 of the 6 states were grouped into two pairs (state 2 and state 3; state 5 and state 6). Abbreviations: L: left; R: right; a: anterior; p: posterior.

state using the Mann–Whitney U test for inter-group comparisons. The decreased transition probabilities from state 1 to states 2 and 3 to state 1 were discovered in IGE compared with HCs ($T_{\text{state } 1\to 2}$: $z = -2.62$, $p = 0.009$; $T_{\text{state } 3\to 1}$: $z = -3.01$, $p = 0.003$). In contrast, an increased probability of

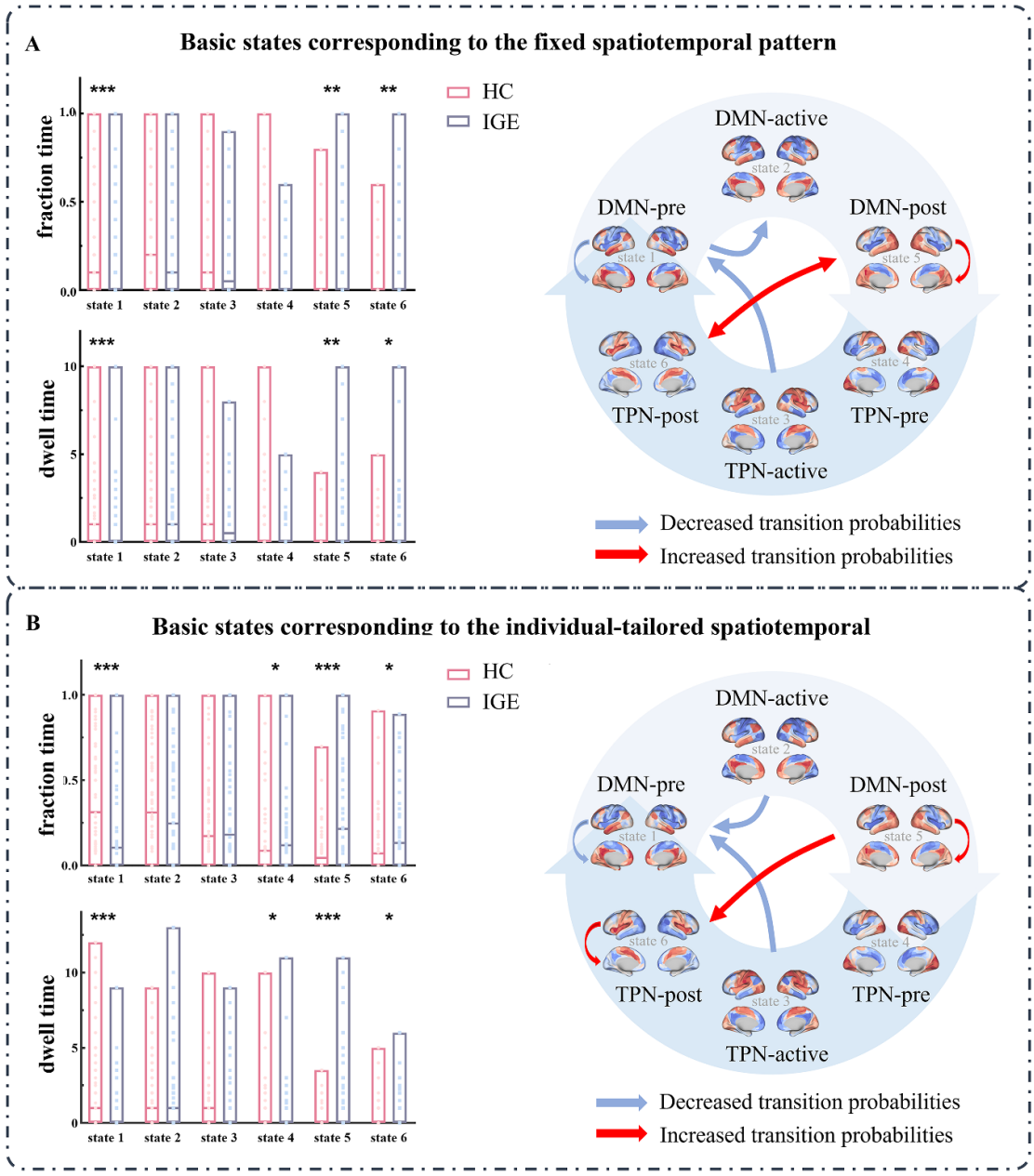

Figure 6. The characteristics of basic states of the brain. (A) The results correspond to the fixed periodic spatiotemporal pattern (PSTP). (B) The features correspond to the individual-tailored PSTP. The first column was the result of fraction time and dwell time, while the second column was the transition probabilities between the six basic states. From a time-domain perspective, the six states depicted different moments of the default mode network (DMN) and task-positive network (TPN) based on the propagation pattern of DMN to TPN in PSTP. Among them, state 2 represented the most active state of DMN (DMN-active); states 1 and 5 represented the states before and after the moment of the DMN-active, namely DMN-pre and DMN-post, respectively. Similarly, state 3 represented the most active state of TPN (TPN-active); states 4 and 6 represented the states before and after the moment of the TPN-active, namely TPN-pre and TPN-post, respectively. Notes: * $p < 0.05$; ** $p < 0.01$; *** $p < 0.001$.

mutual transition was found between states 5 and 6 ($T_{\text{state } 5\to6}$: $z = 2.85$, $p = 0.004$; $T_{\text{state } 6\to5}$: $z = 3.28$, $p = 0.001$) in IGE. The transition probability from a certain state to itself, also known as self-transition probability or self-resilience, is caused by the continuous appearance of this state, indicating that this state is relatively stable in PSTP. In IGE, the self-resilience in state 1 decreased ($T_{\text{state } 1\to1}$: $z = -3.00$, $p = 0.003$), while the resilience in state 5 increased ($T_{\text{state } 5\to5}$: $z = 3.55$, $p < 0.001$).

The results of individual-tailored PSTPs were similar (figure 6(B)). On this basis, this study also observed increased time fractions and dwell times in state 4 ($f_{\text{state } 4}$: $z = 2.30$, $p = 0.021$; $d_{\text{state } 4}$: $z = 2.29$, $p = 0.022$). Furthermore, the self-resilience of state 6 was increased ($T_{\text{state } 6\to6}$: $z = 2$, $p = 0.045$). Notably, although the previously observed reduction in the transition probability from state 1 to state 2 was no longer significant, the transition probability from state 2 to state 1 decreased ($T_{\text{state } 2\to1}$:

$z = -2.09$, $p = 0.037$). Between states 5 and 6, only the probability of the former to the latter increased ($T_{\text{state } 5\to 6}$: $z = 2.15$, $p = 0.031$). In addition, this study also conducted supplementary analyses with $K = 4$ and $K = 5$. When $K = 4$, it was observed that only the self-transition probability of DMN-active in IGE decreased, along with a reduced transition probability between polar states, while no changes in transition probabilities between intermediate states were identified (see supplementary material, figure S6). Nevertheless, when $K = 5$, the results were consistent with those observed for $K = 6$ (figure S7).

3.4. PSTP validation and comparison with traditional approaches

To verify that the observed PSTP originates from the intrinsic temporal structure of the data rather than random statistical phenomena, a surrogate dataset was simulated. The results showed that once the temporal structure was disrupted, the fixed PSTP no longer exhibited a periodic pattern (supplementary material, figure S8). Moreover, none of the individual-tailored PSTPs across subjects achieved stable convergence iterative process failed to terminate (see methods section 2.4.4).

Additionally, in HC, both the fixed and individual-tailored PSTPs demonstrated reduced frequency (fixed PSTP: $z = -8.11$, $p < 0.001$; individual-tailored PSTP: $z = -7.45$, $p < 0.001$), but exhibited higher strength (fixed PSTP: $z = 5.81$, $p < 0.001$; individual-tailored PSTP: $z = 5.87$, $p < 0.001$) and longer interval time (fixed PSTP: $z = 8.06$, $p < 0.001$; individual-tailored PSTP: $z = 7.38$, $p < 0.001$) compared to the original quasi-periodic pattern (Wilcoxon signed rank test). Similar changes were observed in IGE (fixed PSTP: frequency: $z = -7.52$, $p < 0.001$; strength: $z = 5.81$, $p < 0.001$; interval: $z = 8.06$, $p < 0.001$; individual-tailored PSTP: frequency: $z = -7.31$, $p < 0.001$; strength: $z = 6.09$, $p < 0.001$; interval: $z = 7.31$, $p < 0.001$). Despite these within-group changes following algorithm refinement, the between-group differences remained consistent with those identified using PSTP. The quasi- PSTPs of IGE patients consistently exhibited higher strength and interval, and lower frequency than HC (Mann–Whitney U test, $p < 0.05$). Results based on the original algorithm were presented in figure S9.

The traditional sliding window method was also employed to examine the anti-correlation pattern between the DMN and TPN. However, regardless of the window length used (10 TRs or 50 TRs), this approach captured only slow fluctuations between the networks, lacking a discernible periodic structure and failing to reveal temporally organized patterns (figure S10). Regarding noise robustness, both PSTP and the sliding window method demonstrated high robustness. In the HC group, the periodic length of individual-tailored PSTPs showed no significant change before and after adding noise (Wilcoxon signed rank test, $z = 0.84$, $p = 0.401$). The spatial similarity of fixed PSTPs remained high (mean $r = 0.94$), and the squared signal difference between DMN and TPN within PSTPs was similarly stable ($r = 0.93$). Similarly, the squared signal differences obtained from the sliding window method remained highly consistent before and after noise ($r = 0.99$ for both 10 TRs and 50 TRs; Figure S11).

Group-level comparisons using the Mann–Whitney U test based on the traditional sliding window method revealed a significant increase in DMN-TPN anti-correlation strength in IGE patients ($z = 4.99$, $p < 0.001$). However, no significant differences were observed in the frequency ($z = -1.89$, $p = 0.059$) or interval time ($z = 1.94$, $p = 0.053$) of the anti-correlation events (figure S12).

3.5. Stability of findings across different time series lengths

This study verified the reliability of basic states of the brain corresponding to the fixed PSTP by halving the length of the timeseries and gradually increasing the length of the time series. The mean correlation of all states at each time series length was greater than 0.6, as shown in supplementary figure S13.

4. Discussion

The study aimed to investigate the PSTP in spontaneous BOLD signals to characterize individualized rhythmic dynamics in patients with IGE. This is the first study to explore periodic patterns and basic states in IGE across temporal and spatial dimensions. The study revealed four main findings. First, robust individual-tailored PSTPs were identified in HC. Second, DMN-TPN anti-correlation was abnormally decreased during TPN-dominant state in IGE. Additionally, the correlations between the period length of the PSTP and INT were reduced in higher-order cognitive regions, reflecting a diminished capacity of these brain regions to sustain information. Finally, IGE patients showed greater dynamic instability, as indicated by more frequent transitions between transitional states. In summary, these findings offer new insights into the aberrant intrinsic brain activity in IGE and indicate that PSTP analysis is a promising approach for understanding the disease.

4.1. Robust PSTPs and the basic states of the brain

The PSTP reflects a dynamic balance of activation and deactivation between the DMN and TPN, consistent with previously reported quasi- PSTPs [19]. Notably, this study identified robust individual-tailored PSTPs with subject-specific period lengths. The periodic length reflects the dynamic switching between the DMN and TPN, while the INT indicates the timescale of information processing in brain regions [34]. In HC, the positive correlation between period length

and INT was observed mainly in cognitive regions, suggesting that the periodic regulation in cognitive regions is closely linked to their information integration functions. Furthermore, this study simulated surrogate datasets and found that the datasets failed to reproduce individual-tailored PSTP, suggesting that the observed PSTP depends on the intrinsic temporal structure rather than being a spurious pattern. This study also demonstrated its robustness to Gaussian noise [42]. PSTP outperformed the traditional sliding window method in temporal resolution, directly capturing the DMN-TPN anti-correlation dynamics that were obscured by window-averaging effects [43].

An interesting question is whether there is a spatially invariant basis for dynamic behavior between brain regions in PSTP. This study identified six robust basic brain states. Meanwhile, the basic states separated the large-scale networks at rest. In different distributed networks, the time processes of basic states were related to BOLD activation. Furthermore, previous studies have shown that DMN and TPN consistently exhibit strong anti-correlation activity at rest and are associated with cognitive changes [27, 44]. The current findings further reveal that DMN-active and TPN-active represent the most active and inactive poles of DMN, respectively, and play an important role in the transition between brain states. DMN-active was the most common state in healthy subjects, capturing the standard 'static' (time-averaged) task-positive/negative modes, and separating the sensory-motor-attention network from the DMN and LN [40]. The remaining four transition states indicate the signal changes of BOLD propagation from DMN to TPN.

4.2. Disrupted PSTP in IGE patients

PSTPs in IGE patients showed disrupted DMN-TPN dynamics compared to controls. Specifically, the anti-correlation between DMN and TPN was decreased during TPN-dominant states and increased during DMN-ascending states. Although prior studies identified elevated DMN-TPN connectivity and heightened temporal variability in GTCS [45, 46], these analyses primarily relied on averaged time series or modular approaches that focused separately on temporal or spatial domains [47, 48]. The PSTP of this study extends these results, providing a complementary explanation in the spatiotemporal domain. The current study results demonstrate that DMN dysfunction in IGE exhibits state-dependence, with a direct association to abnormal BOLD phase transitions. This also suggests the interruption or enhancement of FC in IGE might at least partially reflect the dysfunction in processes that create spatiotemporal patterns. Notably, the intermittent breakdowns of the anti-correlation could interfere with the functional and structural disintegration of the cortical network, potentially contributing to recurrent abnormal discharges in epilepsy [49]. Future work could use synchronous EEG-fMRI to explore the relationship between anti-correlation dynamics across PSTP states and epileptic discharges, offering new avenues for seizure prediction and behavioral assessment.

Beyond altered DMN-TPN coupling, the overall PSTP profiles differed between groups. In IGE, PSTP strength was significantly increased, reflecting enhanced anti-correlation signals [20], which may indicate greater recruitment and redistribution of cognitive resources during task-related states. This heightened demand could be linked to impaired behavioral performance [50, 51] and alertness [52] or attentional deficits [53]. Crucially, even when controlling for PSTP frequency, its strength remained elevated in IGE, suggesting a stronger influence on intrinsic brain dynamics. Previous studies established that spatiotemporal patterns contribute to FC, especially within pathology-vulnerable regions [42, 54]. Consistent with earlier findings of DMN dysfunction in IGE [9, 55], static FC analysis revealed increased DMN-TPN connectivity (i.e. reduced anti-correlation). However, these differences disappeared after accounting for PSTPs, underscoring their dominant role in shaping FC alterations. Disruption of PSTPs may thus represent a mechanistic contributor to disease pathophysiology [54]. Future studies on the relationship between PSTPs and FC could enhance understanding of the etiology of IGE. Importantly, PSTP provided a more comprehensive characterization of IGE pathology compared to conventional dFC approaches. This study shows that conventional dFC with a 50 TR window length can only detect between-group differences in DMN-TPN anti-correlation strength. In contrast, PSTP reveals multi-dimensional abnormalities in IGE, further supporting its potential as a disease biomarker.

4.3. Basic states of IGE patient reconfiguration

The patients with IGE tend to remain in transitional states in the current study, particularly DMN-post and TPN-post, indicating that the basic states of IGE patients undergo continuous combination, dissolution, and reorganization to form adaptive activity patterns [56]. The decreased probabilities of transition at two poles indicate dysregulated switching between intrinsic and extrinsic attention in IGE, leading to functional disorganization, compromised cognitive maintenance, and ultimately cognitive dysfunction [45]. Additionally, meta-analysis decoding using Neurosynth [36] revealed that the decreased correlation between period length and INT in IGE patients could reflect deficits in task-related processes such as engagement and retrieval. These results support that abnormal periodic regulation impairs information maintenance in higher-order cognitive regions. Taken together, these findings establish

potential connections between PSTP alterations and cognitive dysfunction in epilepsy.

4.4. Limitations

Several methodological limitations should be noted. First, low-frequency fluctuations may originate from subcortical sources or modulatory 'driving' factors [16], suggesting that subcortical nuclei play a crucial role in shaping PSTPs. Future studies should incorporate subcortical structures to examine their activation patterns and contributions to epilepsy pathophysiology. Second, given that antiseizure medications can significantly alter brain activity, this study used the Kruskal–Wallis test ($p < 0.05$) to compare the strength, frequency, and interval time of PSTP across HC, medicated patients, and drug-naïve first-episode patients. Post hoc analyses were conducted using the Mann–Whitney U test ($p < 0.05$). The results showed no significant differences between drug-naïve and medicated patients. Moreover, both patient groups showed similar alterations compared to HCs (supplementary tables S1 and S2). However, potential confounds remain: variation in medication type, dosage, and treatment duration was not controlled, and antiseizure medications may exert subtle effects on network dynamics not captured here. Future work should adopt controlled longitudinal or pharmacological designs to characterize the impact of antiseizure medications more precisely on PSTP.

5. Conclusion

This study proposed a novel tool to identify PSTPs in patients with IGE, demonstrating abnormal dynamic rhythms across temporal and spatial domains. The attenuated DMN-TPN anti-correlation during the TPN-dominant states suggests disrupted network switching and a loss of functional balance. The observed increased PSTP strength in IGE points to heightened reliance on periodic activity patterns, potentially compromising network regulation and contributing to cognitive deficits. Furthermore, the weakened correlations between period length and INT in higher-order cognitive regions imply diminished information integration capacity. IGE patients exhibited a propensity for flexible transitions between transitional states. Together, these findings provide new insights into the pathophysiological mechanisms of IGE, offering potential directions for future research on epilepsy activity generation and spread.

Data availability statement

The data cannot be made publicly available upon publication because they contain sensitive personal information. The data that support the findings of this study are available upon reasonable request from the authors.

Acknowledgment

We thank all the subjects who participated in this study, as well as the researchers and scientific advisors for their valuable contributions to the study design. We are also grateful to our colleagues for their assistance in data collection.

This work was supported by the National Key R&D Program of China (2024YFE0215100), the STI 2030-Major Projects (2022ZD0208500), the National Natural Science Foundation of China (62401124, 62201133, and 82371560), the Natural Science Foundation of Sichuan (2023NSFSC0037), the China Postdoctoral Science Foundation (2021TQ0061), and the CAMS Innovation Fund for Medical Sciences (CIFMS, 2019-I2M-5-039).

CRediT authorship contribution statement

Junxia Chen: Writing—original draft, Software, Formal analysis, Data curation, Conceptualization. **Sisi Jiang:** Writing—review & editing, Methodology, Formal analysis. **Guofeng Ye:** Data curation. **Zhihuan Yang:** Resources, Investigation. **Changyue Hou:** Methodology, Data analysis. **Hechun Li:** Writing—review & editing, Data analysis, Data curation. **Haonan Pei:** Writing—review & editing, Visualization, Data analysis. **Roberto Rodriguez-Labrada:** Draft Revising—review & editing. **Jianfu Li:** Investigation, Data curation. **Dezhong Yao:** Writing—review & editing, Resources. **Cheng Luo:** Draft Writing—review & revising, Conceptualization, Supervision, Resources, Project administration.

Conflict of interest

The authors have no relevant financial or non-financial interests to disclose.

Funding

This work was supported by National Key R&D Program of China, (2024YFE0215100), the STI 2030-Major Projects 2022ZD0208500, the National Nature Science Foundation of China (62401124, 62201133, and 82371560), the Natural Science Foundation of Sichuan (2023NSFSC0037) China Postdoctoral Science Foundation (2021TQ0061), and the CAMS Innovation Fund for Medical Sciences (CIFMS) (No.2019-I2M-5-039).

Code availability statement

Scripts for exploring periodic spatiotemporal patterns can be accessed at GitHub (https://github.com/joysober/Detect-PSTP). The pseudocode was provided in supplementary material.

The relationship between RSTP, RRP, and PSTP

The repeated spatiotemporal pattern (RSTP), representative repeated pattern (RRP), and periodic spatiotemporal pattern (PSTP) were all four-dimensional spatiotemporal patterns representing repeated fragments in BOLD signals. This study aimed to identify a stable PSTP. First, multiple RSTPs were identified for each participant using the pattern-finding algorithm (Step 01: Detection of Repeated Spatiotemporal Patterns). Next, the RRP closest to a DMN-to-TPN transition was selected from RSTPs (Step 02: Searching for Representative Repeated Pattern). Then, the period length of the RRP was calculated (Step 03: Definition of Period Length of the RRP). Finally, the parameter W (the number of timepoints forming each RSTP) was optimized based on the period length. An iterative algorithm was applied to refine the RRP under varying parameters until the period length stabilized between consecutive RRPs. The final stabilized RRP was defined as the PSTP (Step 04: Robust PSTP detection).

ORCID iDs

Junxia Chen 0009-0000-8643-1298
Guofeng Ye 0009-0002-7179-4488
Roberto Rodriguez-Labrada 0000-0003-3193-7683
Jianfu Li 0000-0001-5555-3639
Dezhong Yao 0000-0002-8042-879X

References

[1] Hirsch E *et al* 2022 ILAE definition of the idiopathic generalized epilepsy syndromes: position statement by the ILAE task force on nosology and definitions *Epilepsia* **63** 1475–99
[2] Ren X, Brodovskaya A, Hudson J L and Kapur J 2021 Connectivity and neuronal synchrony during seizures *J. Neurosci.* **41** 7623–35
[3] Dhaher R *et al* 2021 Network-related changes in neurotransmitters and seizure propagation during rodent epileptogenesis *Neurology* **96** E2261–71
[4] Shahabi H, Nair D R, Leahy R M and Fornito A 2023 Multilayer brain networks can identify the epileptogenic zone and seizure dynamics *Elife* **12** e68531
[5] Gelinas J N and Khodagholy D 2025 Interictal network dysfunction and cognitive impairment in epilepsy *Nat. Rev. Neurosci.* **26** 399–414
[6] Gotman J, Grova C, Bagshaw A, Kobayashi E, Aghakhani Y and Dubeau F 2005 Generalized epileptic discharges show thalamocortical activation and suspension of the default state of the brain *Proc. Natl Acad. Sci. USA* **102** 15236–40
[7] Li Y X, Ran Y, Yao M H and Chen Q 2024 Altered static and dynamic functional connectivity of the default mode network across epilepsy subtypes in children: a resting-state fMRI study *Neurobiol. Dis.* **192** 106425
[8] Yang S Q *et al* 2021 Temporal variability profiling of the default mode across epilepsy subtypes *Epilepsia* **62** 61–73
[9] Liu F, Wang Y F, Li M L, Wang W Q, Li R, Zhang Z Q, Lu G M and Chen H F 2017 Dynamic functional network connectivity in idiopathic generalized epilepsy with generalized tonic-clonic seizure *Hum. Brain Mapp.* **38** 957–73
[10] Caciagli L and Bassett D S 2022 Epilepsy imaging meets machine learning: a new era of individualized patient care *Brain* **145** 807–10
[11] Jiang L-W, Qian R-B, Fu X-M, Zhang D, Peng N, Niu C-S and Wang Y-H 2018 Altered attention networks and DMN in refractory epilepsy: a resting-state functional and causal connectivity study *Epilepsy Behav.* **88** 81–86
[12] Fajardo-Valdez A, Camacho-Téllez V, Rodríguez-Cruces R, García-Gomar M L, Pasaye E H, Concha L and Fischmeister F P S 2024 Functional correlates of cognitive performance and working memory in temporal lobe epilepsy: insights from task-based and resting-state fMRI *PLoS One* **19** e0295142
[13] Zhang Z, Zhou X, Liu J P, Qin L, Ye W and Zheng J N 2020 Aberrant executive control networks and default mode network in patients with right-sided temporal lobe epilepsy: a functional and effective connectivity study *Int. J. Neurosci.* **130** 683–93
[14] Yuan Y, Duan Y, Li W, Ren J C, Li Z M and Yang C L 2023 Differences in the default mode network of temporal lobe epilepsy patients detected by hilbert-huang transform based dynamic functional connectivity *Brain Topogr.* **36** 581–94
[15] Donoghue T *et al* 2020 Parameterizing neural power spectra into periodic and aperiodic components *Nat. Neurosci.* **23** 1655–65
[16] Drew P J, Duyn J H, Golanov E and Kleinfeld D 2008 Finding coherence in spontaneous oscillations *Nat. Neurosci.* **11** 991–3
[17] Drew P J, Mateo C, Turner K L, Yu X and Kleinfeld D 2020 Ultra-slow oscillations in fMRI and resting-state connectivity: neuronal and vascular contributions and technical confounds *Neuron* **107** 782–804
[18] Gu H, Schulz K P, Fan J and Yang Y H 2021 Temporal dynamics of functional brain states underlie cognitive performance *Cereb. Cortex* **31** 2125–38
[19] Yousefi B and Keilholz S 2021 Propagating patterns of intrinsic activity along macroscale gradients coordinate functional connections across the whole brain *Neuroimage* **231** 117827
[20] Thompson G J, Pan W-J, Magnuson M E, Jaeger D and Keilholz S D 2014 Quasi-periodic patterns (QPP): large-scale dynamics in resting state fMRI that correlate with local infraslow electrical activity *Neuroimage* **84** 1018–31
[21] Grooms J K, Thompson G J, Pan W-J, Billings J, Schumacher E H, Epstein C M and Keilholz S D 2017 Infraslow electroencephalographic and dynamic resting state network activity *Brain Connect.* **7** 265–80
[22] Qin L, Zhou Q, Sun Y T, Pang X M, Chen Z R and Zheng J N 2024 Dynamic functional connectivity and gene expression correlates in temporal lobe epilepsy: insights from hidden markov models *J. Transl. Med.* **22** 763
[23] Ke M, Hou L and Liu G Y 2024 The co-activation patterns of multiple brain regions in Juvenile Myoclonic Epilepsy *Cogn. Neurodyn.* **18** 337–47
[24] Huckins G and Poldrack R A 2024 Generative dynamical models for classification of rsfMRI data *Netw. Neurosci.* **8** 1613–33
[25] Matsui T, Pham T Q, Jimura K and Chikazoe J 2022 On co-activation pattern analysis and non-stationarity of resting brain activity *Neuroimage* **249** 118904
[26] Dosenbach N U, Raichle M E and Gordon E M 2025 The brain's action-mode network *Nat. Rev. Neurosci.* **26** 158–68
[27] Menon V 2023 20 years of the default mode network: a review and synthesis *Neuron* **111** 2469–87
[28] Raichle M E 2015 The brain's default mode network *Annu. Rev. Neurosci.* **38** 433–47
[29] Yu Y, Wang H D, Liu X T and Wang Q Y 2024 Closed-loop transcranial electrical stimulation for inhibiting epileptic

activity propagation: a whole-brain model study *Nonlinear Dyn.* **112** 21369–87
[30] Scheffer I E *et al* 2017 ILAE classification of the epilepsies: position paper of the ILAE commission for classification and terminology *Epilepsia* **58** 512–21
[31] Esteban O *et al* 2019 fMRIPrep: a robust preprocessing pipeline for functional MRI *Nat. Methods* **16** 111–6
[32] Glasser M F *et al* 2016 A multi-modal parcellation of human cerebral cortex *Nature* **536** 1718
[33] Yeo B T *et al* 2011 The organization of the human cerebral cortex estimated by intrinsic functional connectivity *J. Neurophysiol.* **106** 1125–65
[34] Wolff A, Berberian N, Golesorkhi M, Gomez-Pilar J, Zilio F and Northoff G 2022 Intrinsic neural timescales: temporal integration and segregation *Trends Cognit. Sci.* **26** 159–73
[35] Raut R V, Snyder A Z and Raichle M E 2020 Hierarchical dynamics as a macroscopic organizing principle of the human brain *Proc. Natl Acad. Sci. USA* **117** 20890–7
[36] Yarkoni T, Poldrack R A, Nichols T E, Van Essen D C and Wager T D 2011 Large-scale automated synthesis of human functional neuroimaging data *Nat. Methods* **8** 665–70
[37] Honari H, Choe A S and Lindquist M A 2021 Evaluating phase synchronization methods in fMRI: a comparison study and new approaches *Neuroimage* **228** 117704
[38] Lamprou C, Apostolidis G, Alshehhi A, Hadjileontiadis L J and Seghier M L 2025 Robust fMRI time-varying functional connectivity analysis using multivariate swarm decomposition *Neurocomputing* **642** 130404
[39] Cabral J, Vidaurre D, Marques P, Magalhaes R, Silva Moreira P, Miguel Soares J, Deco G, Sousa N and Kringelbach M L 2017 Cognitive performance in healthy older adults relates to spontaneous switching between states of functional connectivity during rest *Sci. Rep.* **7** 5135
[40] Favaretto C, Allegra M, Deco G, Metcalf N V, Griffis J C, Shulman G L, Brovelli A and Corbetta M 2022 Subcortical-cortical dynamical states of the human brain and their breakdown in stroke *Nat. Commun.* **13** 5069
[41] Glasser M F *et al* 2013 The minimal preprocessing pipelines for the human connectome project *Neuroimage* **80** 105–24
[42] Abbas A, Belloy M, Kashyap A, Billings J, Nezafati M, Schumacher E H and Keilholz S 2019 Quasi-periodic patterns contribute to functional connectivity in the brain *Neuroimage* **191** 193–204
[43] Vergara V M, Abrol A and Calhoun V D 2019 An average sliding window correlation method for dynamic functional connectivity *Hum. Brain Mapp.* **40** 2089–103
[44] Watters H, Fazili A, Daley L, Belden A, LaGrow T, Bolt T, Loui P and Keilholz S 2024 Creative tempo: spatiotemporal dynamics of the default mode network in improvisational musicians *bioRxiv Preprint* https://doi.org/10.1101/2024.04.07.588391
[45] Jia X Y *et al* 2020 Reconfiguration of dynamic large-scale brain network functional connectivity in generalized tonic-clonic seizures *Hum. Brain Mapp.* **41** 67–79
[46] Pei H *et al* 2022 Functional and structural networks decoupling in GTCS and its reorganization by drugs (https://doi.org/10.1002/epi4.12781)
[47] Jiang S, Li H, Liu L, Yao D and Luo C 2022 Voxel-wise functional connectivity of the default mode network in epilepsies: a systematic review and meta-analysis *Curr. Neuropharmacol.* **20** 254–66
[48] Mohan A, Roberto A J, Mohan A, Lorenzo A, Jones K, Carney M J, Liogier-Weyback L, Hwang S and Lapidus K A 2016 The significance of the default mode network (DMN) in neurological and neuropsychiatric disorders: a review *Yale J. Biol. Med.* **89** 49–57 (available at: https://pmc.ncbi.nlm.nih.gov/articles/PMC4797836/)
[49] Goodman A M and Szaflarski J P 2021 Recent advances in neuroimaging of epilepsy *Neurotherapeutics* **18** 811–26
[50] Patrikelis P *et al* 2022 Selective impairment of auditory attention processing in idiopathic generalized epilepsies: implications for their cognitive pathophysiology *Appl. Neuropsychol. Adult.* **29** 1131–40
[51] Chou T A, Dougherty D D, Nierenberg A A and Deckersbach T 2022 Restoration of default mode network and task positive network anti-correlation associated with mindfulness-based cognitive therapy for bipolar disorder *Psychiatry Res. Neuroimaging* **319** 111419
[52] Gattuso J J *et al* 2023 Default mode network modulation by psychedelics: a systematic review *Int. J. Neuropsychopharmacol.* **26** 155–88
[53] Chowdhury F A, Elwes R D C, Koutroumanidis M, Morris R G, Nashef L and Richardson M P 2014 Impaired cognitive function in idiopathic generalized epilepsy and unaffected family members: an epilepsy endophenotype *Epilepsia* **55** 835–40
[54] Abbas A, Bassil Y and Keilholz S 2019 Quasi-periodic patterns of brain activity in individuals with attention-deficit/hyperactivity disorder *NeuroImage Clin.* **21** 101653
[55] Espinosa J, Alves K and Betting L 2021 Modulation of resting state networks by antiseizure medications in patients with idiopathic generalized epilepsy *Neurology* **96** 4886
[56] Jiang S S, Pei H N, Huang Y, Chen Y, Liu L L, Li J F, He H, Yao D Z and Luo C 2020 Dynamic temporospatial patterns of functional connectivity and alterations in idiopathic generalized epilepsy *Int. J. Neural Syst.* **30** 2050065